



## Abstract

The sedimentation of  $\text{HNO}_3$  containing Polar Stratospheric Cloud (PSC) particles leads to a permanent removal of  $\text{HNO}_3$  and thus to a denitrification of the stratosphere, an effect which plays an important role in stratospheric ozone depletion. The polar vortex in the Arctic winter 2009/2010 was very cold and stable between end of December and end of January. Strong denitrification was observed in the Arctic in mid of January by the Odin Sub Millimetre Radiometer (Odin/SMR) which was the strongest denitrification that had been observed in the entire Odin/SMR measuring period (2001–2010). Lidar measurements of PSCs were performed in the area of Kiruna, Northern Sweden with the IRF (Institutet för Rymdfysik) lidar and with the Esrange lidar in January 2010. The measurements show that PSCs were present over the area of Kiruna during the entire period of observations. The formation of PSCs during the Arctic winter 2009/2010 is investigated using a microphysical box model. Box model simulations are performed along air parcel trajectories calculated six days backward according to the PSC measurements with the ground-based lidar in the Kiruna area. From the temperature history of the trajectories and the box model simulations we find two PSC regions, one over Kiruna according to the measurements made in Kiruna and one north of Scandinavia which is much colder, reaching also temperatures below  $T_{\text{ice}}$ . Using the box model simulations along backward trajectories together with the observations of Odin/SMR, CALIPSO (Cloud-Aerosol Lidar and Infrared Pathfinder Satellite Observations) and the ground-based lidar we investigate how and by which type of PSC particles the denitrification that was observed during the Arctic winter 2009/2010 was caused. From our analysis we find that due to an unusually strong synoptic cooling event in mid January, ice particle formation on NAT may be a possible mechanism that caused denitrification during the Arctic winter 2009/2010.

### Denitrification and polar stratospheric cloud formation

F. Khosrawi et al.

Title Page

Abstract

Introduction

Conclusions

References

Tables

Figures



Back

Close

Full Screen / Esc

Printer-friendly Version

Interactive Discussion



## 1 Introduction

Polar stratospheric clouds (PSC) play a key role in stratospheric ozone destruction in the polar regions (Solomon et al., 1986; Crutzen and Arnold, 1986). Heterogeneous reactions which take place on and within the PSC particles convert halogens from relatively inert reservoir species into forms which can destroy ozone in the polar spring (e.g., Peter, 1997; Solomon, 1999; Lowe and MacKenzie, 2008). PSC occur with different compositions and physical phases and were originally classified according to their occurrence above (type I) and below (type II) the water ice frost point ( $T_{ice}$ ) (McCormick et al., 1982; Poole and McCormick, 1988). Later, type I PSCs were sub-classified into non-spherical solid particles (type Ia) and spherical liquid particles (type Ib). Trajectory studies reveal that the physical state of sulfate particles and PSCs in the stratosphere is strongly controlled by the temperature history of the air mass (e.g., Tabazadeh et al., 1995; Larsen et al., 1997; Toon et al., 2000). Type Ib PSCs are composed of supercooled ternary solution particles (STS;  $H_2SO_4/H_2O/HNO_3$ ) and are formed by the up-take of  $H_2O$  and  $HNO_3$  on the liquid stratospheric  $H_2SO_4/H_2O$  (background) aerosols at temperatures below  $\approx 193$  K (Carslaw et al., 1994; Meilinger et al., 1995; Peter, 1997; Lowe and MacKenzie, 2008). PSCs Ia particles are composed of nitric acid trihydrate (NAT), the stable  $HNO_3$  hydrate under stratospheric conditions (Toon et al., 1986; Hanson and Mauersberger, 1988) and PSC type II of pure water ice (Steele et al., 1983; Browell et al., 1990). The formation of solid PSC type Ia and II particles is generally assumed to be initiated by the homogeneous freezing of supercooled ternary solution particles at temperatures 3–4 K below the ice frost point  $T_{ice} \approx 185$  K (Koop et al., 1995).

Though from the previous paragraph it seems that PSC formation is quite well understood a lot of uncertainties remain, especially concerning the formation of solid PSCs of type Ia and II. Besides the exact formation mechanism of PSC type Ia and II, it seems that temperatures below  $T_{ice}$  for PSC type Ia formation are not necessarily required (e.g., Toon et al., 2000; Larsen et al., 2002; Drdla and Browell, 2004). In general, homogeneous formation processes have been assumed, but measurements have indicated

### Denitrification and polar stratospheric cloud formation

F. Khosrawi et al.

Title Page

Abstract

Introduction

Conclusions

References

Tables

Figures



Back

Close

Full Screen / Esc

Printer-friendly Version

Interactive Discussion



**Denitrification and  
polar stratospheric  
cloud formation**

F. Khosrawi et al.

Title Page

Abstract

Introduction

Conclusions

References

Tables

Figures

◀

▶

◀

▶

Back

Close

Full Screen / Esc

Printer-friendly Version

Interactive Discussion



that solid PSC particles can also be formed heterogeneously (e.g., Koop et al., 1997; Voigt et al., 2005). Ice freezes out of liquid ternary solutions at temperatures several degrees below the ice frost point if homogeneous freezing is the prevailing formation process (Koop et al., 1995, 2000). If ice particles form heterogeneously according to the three-stage model they will form on NAT particles (Drdla and Turco, 1991). In later studies as e.g. in Peter (1997) these three-stage process has been omitted and it was suggested the vice-versa process namely that NAT particles form on ice (thus at temperatures 3–4 K below  $T_{ice}$ ).

On synoptic scales in the Arctic temperatures 3–4 K below  $T_{NAT}$  occur infrequently whereas NAT particles are often observed in large-scale PSCs (Toon et al., 2000). Large-scale temperature histories indicate that solid PSC have spent several days close to or below the NAT existence temperature ( $T_{NAT} \approx 195$  K) (e.g., Tabazadeh et al., 1996; Larsen et al., 1997; Larsen et al., 2002). The exact NAT formation mechanism is still under debate and different NAT formation mechanism have been suggested. Laboratory measurements (e.g., Salcedo et al., 2001) show that the homogeneous nucleation of NAT and NAD (nitric acid dihydrate) in STS droplets is too slow under stratospheric conditions to explain high NAT particle concentrations ( $>10^{-1}$  cm $^{-3}$ ) observed in mountain wave PSCs (e.g., Voigt et al., 2000; Pitts et al., 2011). Moreover, Knopf et al. (2002) show that homogeneous nucleation of NAT/NAD cannot even explain the lowest observed NAT number densities of  $10^{-4}$  cm $^{-3}$  (Fahey et al., 2001). Measurements by Zondlo et al. (2000) indicate that also heterogeneous NAT nucleation from binary HNO $_3$ /H $_2$ O solution on an ice surface does not rapidly occur, but forms a metastable HNO $_3$ -H $_2$ O film. Instead, NAT nucleation by vapour deposition onto ice surfaces has been observed to proceed at high NAT supersaturation (e.g., Biermann et al., 1998). Further, Voigt et al. (2005) suggested meteoric smoke particles for triggering heterogeneous NAT nucleation.

Solid PSC particles can grow to larger sizes than liquid PSC particles and finally sediment out of the stratosphere (Fahey et al., 2001). The sedimentation of the solid particles can lead either to a dehydration or a denitrification of the stratosphere. The

**Denitrification and  
polar stratospheric  
cloud formation**

F. Khosrawi et al.

Title Page

Abstract

Introduction

Conclusions

References

Tables

Figures

◀

▶

◀

▶

Back

Close

Full Screen / Esc

Printer-friendly Version

Interactive Discussion



sedimentation of large nitric acid ( $\text{HNO}_3$ ) containing particles leads to an irreversible removal of  $\text{HNO}_3$  and thus limits the deactivation process in springtime allowing the ozone-destroying catalytic cycle to last longer. Denitrification cannot be explained by the sedimentation of liquid PSC particles. The available nitric acid is distributed on all particles in the background size distribution during condensation, thus preventing the formation of large liquid particles with significant fall speeds (Larsen et al., 2002). Further, denitrification is in the Arctic usually observed without concurrent dehydration (Fahey et al., 1990), making it difficult to explain Arctic denitrification by falling ice particles with inclusion of nitric acid. Fahey et al. (2001) suggested that Arctic denitrification could be caused by a selective, but yet unknown, nucleation mechanism responsible for the formation of a small number of large solid particles as was first observed in the 1999/2000 Arctic winter stratosphere. However, during cold Arctic winters dehydration has been observed in the Arctic (e.g., Fahey et al., 1990; Ovarlez and Ovarlez, 1994; Vömel et al., 1997), thus making the process of ice formation on NAT particles and subsequent sedimentation that causes denitrification possible during such winters. Further, in a recent study by Pitts et al. (2011) analysing CALIPSO (Cloud-Aerosol Lidar and Infrared Pathfinder Satellite Observations) observations for the Arctic winter 2009/2010 an increase of ice observations with a coincident decrease in NAT mixtures under a synoptic-scale cooling event was observed, suggesting that under these conditions heterogeneous nucleation on NAT particles may be an important process for ice PSC formation.

Here, we investigate PSC formation and denitrification during the Arctic winter 2009/2010 applying ground-based and satellite-borne measurements in combination with microphysical box model simulations. Measurements of  $\text{HNO}_3$  derived from Odin/SMR (Odin Sub-Millimetre Radiometer) are applied to investigate denitrification. PSC are investigated using satellite measurements from CALIPSO and ground-based measurements from two lidars in the area of Kiruna, Northern Sweden, one located at Esrange ( $67.8^\circ \text{N}$ ,  $21.1^\circ \text{E}$ ) and one located at IRF ( $67.8^\circ \text{N}$ ,  $20.4^\circ \text{E}$ ). The ground-based measurements with the lidar instruments were performed in the frame of the

European research project RECONCILE (reconciliation of essential parameters for an enhanced predictability of Arctic stratospheric ozone loss and its climate interactions), an intensive field campaign with the M55-Geophysica research aircraft. The RECONCILE campaign was performed during January–March 2010 (von Hobe et al., 2011).

## 2 Instrumentation and model description

### 2.1 Odin/SMR

The Odin satellite was launched on 20 February 2001 and has thus been in operation now for almost 10 years. Odin is operated by the Swedish Space cooperation in collaboration with groups from France, Canada and Finland (Murtagh et al., 2002). The Sub-Millimetre Radiometer (SMR) on board the Odin satellite observes the thermal emission from the Earth limb. Vertical profiles of trace gases such as O<sub>3</sub>, ClO, N<sub>2</sub>O, HNO<sub>3</sub>, H<sub>2</sub>O, CO and NO, as well as of isotopes of H<sub>2</sub>O and O<sub>3</sub> are measured (Murtagh et al., 2002). Measurements are generally performed in the altitude range from 7 to 70 km with a resolution of  $\approx 1.5$  km in terms of tangent altitude below 50 km and  $\approx 5.5$  km above. Usually, the latitude range between 83.5° S and 82.5° N is covered by the measurements (Urban et al., 2005).

Here, we use measurements of HNO<sub>3</sub> from Odin/SMR originating from the band centered at 544.6 GHz. HNO<sub>3</sub> volume mixing ratios are retrieved above 18–19 km up to  $\approx 45$  km. The single profile precision is 1 ppbv (corresponding to 10–15% below 30 km) and the resolution in altitude is 1.5–2 km, degrading with increasing altitude, e.g.  $\approx 3$  km at 35 km (Urban et al., 2009). The horizontal resolution is 300 km determined by the limb path in the tangent layer. The systematic error of Odin/SMR HNO<sub>3</sub> measurements has been estimated to be better than 0.7 ppbv (Urban et al., 2005). However, a larger positive bias of the order 2–3 ppbv ( $\approx 20\%$ ) was found by comparison with other satellite instrument like e.g. MLS (Microwave Limb Sounder) on Aura, ACE-FTS (Atmospheric Fourier Transform Spectrometer) on SCISAT-1 and MIPAS (Michelson

## Denitrification and polar stratospheric cloud formation

F. Khosrawi et al.

Title Page

Abstract

Introduction

Conclusions

References

Tables

Figures

◀

▶

◀

▶

Back

Close

Full Screen / Esc

Printer-friendly Version

Interactive Discussion



Interferometer for Passive Atmospheric Soundings) on ENVISAT (e.g., Urban et al., 2006). In the Odin/SMR v2.0 HNO<sub>3</sub> data used here the bias has been accounted for applying an empirical linear scaling correction as described in Urban et al. (2009). Corrected HNO<sub>3</sub> mixing ratios were found to be within 0.5 ppbv of those of coincident ACE/FTS measurements (v2.2 data).

## 2.2 CALIPSO

CALIPSO (Cloud-Aerosol Lidar and Infrared Pathfinder Satellite Observations) is part of the NASA/ESA “A-Train” satellite constellation and has been in operation since June 2006. Measurements of polar stratospheric clouds (PSCs) are provided by CALIOP (Cloud-Aerosol Lidar with Orthogonal Polarization) on board of CALIPSO. CALIOP is a two-wavelength, polarization sensitive lidar. High vertical resolution profiles of the backscatter coefficient at 532 and 1064 nm as well as two orthogonal (parallel and perpendicular) polarization components at 532 nm are provided (Winker et al., 2007; Pitts et al., 2007). The lidar pulse rate is 20.25 Hz, corresponding to one profile every 333 m. The vertical resolution of CALIOP varies with altitude from 30 m in the lower troposphere to 180 m in the stratosphere. The determination of the composition of PSCs is based on the measured aerosol depolarization ratio (ratio of parallel and perpendicular components of 532-nm backscatter) and the inverse scattering ratio ( $1/R_{532}$ ), where  $R_{532}$  is the ratio of the total to molecular backscatter at 532 nm (Pitts et al., 2007, 2009). Using these two quantities, PSCs are classified into: STS, water ice, and three classes of liquid/NAT mixtures (Mix 1, Mix 2 and Mix 2 enhanced). Mix 1 denotes mixtures with very low NAT number densities (from about  $3 \times 10^{-4} \text{ cm}^{-3}$  to  $10^{-3} \text{ cm}^{-3}$ ), Mix 2 denotes mixtures with intermediate NAT number densities of ( $10^{-3} \text{ cm}^{-3}$ ), and Mix 2-enhanced denotes mixtures with sufficiently high NAT number densities ( $>0.1 \text{ cm}^{-3}$ ) and volumes ( $>0.5 \mu\text{m}^3 \text{ cm}^{-3}$ ) that their presence is not masked by the more numerous STS droplets at temperatures well below  $T_{\text{NAT}}$ . In addition, intense mountain-wave induced ice PSCs are identified as a subset of CALIPSO ice PSCs through their distinct optical signature in  $R_{532}$  (Pitts et al., 2011).

## Denitrification and polar stratospheric cloud formation

F. Khosrawi et al.

Title Page

Abstract

Introduction

Conclusions

References

Tables

Figures



Back

Close

Full Screen / Esc

Printer-friendly Version

Interactive Discussion



## 2.3 Esrange and IRF lidar

Lidar measurements were performed in the area of Kiruna at Esrange with the Esrange lidar (67.8° N, 21.1° E) and at IRF with the IRF lidar (67.8° N, 20.4° E). The Esrange lidar has been operated since 1997 while the IRF lidar started its operation in 2005.

5 The Esrange lidar is a RMR (Rayleigh/Mie/Raman) lidar while the IRF lidar utilizes a conventional backscatter lidar technique only. Both lidar use a pulsed Nd:YAG solid-state laser as transmitter. Short light pulses of 10 ns in length are emitted with 20 and 30 Hz, respectively. Measurements are performed at 532-nm wavelength in two orthogonal polarisation directions. The backscattered light is collected by telescope  
10 systems, split according to its linear state of polarisation, detected by photomultipliers and recorded by counting electronics. The elapsed time between the emission of a light pulse and the detection of the backscatter signal determines the scattering altitude. The sum of the backscattered light of molecules and aerosols is detected by the lidar. To determine the molecular fraction of the received signal ( $I_{\text{mol}}$ , the signal of the  $\text{N}_2$ -vibrational Raman scattered light is scaled to the raw signal above the PSC (Blum and Fricke, 2005). The intensities of the different channels ( $I_{\text{mol}}$ ,  $I_{\text{par}}$ ,  $I_{\text{perp}}$ ) are used to derive quantities like backscatter ratio  $R$ , the aerosol backscatter coefficient  $\beta_{\text{aer}}$  and the aerosol depolarization  $\delta_{\text{aer}}$  (Blum et al., 2005, 2006). From the backscatter ratio and the backscatter coefficient the amount of aerosol is determined. From the  
20 depolarisation it is determined whether the aerosol particles are spherical which allows to distinguish between liquid and solid aerosol particles. Using the backscatter and depolarisation derived from measurements performed with the Esrange lidar between 1997–2004, a classification scheme has been developed to distinguish between NAT, STS and ice particles (Blum et al., 2005). Since the classification scheme does not  
25 cover all PSC measurements, the remaining data points are assumed to be mixed clouds, containing a strong and a weak depolarizing scatterer as NAT or STS. PSC classification for the IRF lidar is done according to Browell et al. (1990) and Blum et al. (2005). Measurements with the Esrange lidar are performed in the altitude range from

### Denitrification and polar stratospheric cloud formation

F. Khosrawi et al.

Title Page

Abstract

Introduction

Conclusions

References

Tables

Figures



Back

Close

Full Screen / Esc

Printer-friendly Version

Interactive Discussion



10–80 km with a vertical resolution of 150 m while measurements with the IRF lidar are performed between 10–50 km with a vertical resolution of 30 m.

## 2.4 Microphysical box model

The formation of liquid PSCs of type 1b (STS) was simulated along backward trajectories with a microphysical box model. The microphysical box model has previously been successfully applied for different kinds of aerosol formation and growth studies in the upper troposphere (e.g., Khosrawi and Konopka, 2003; Khosrawi et al., 2010) as well as for case studies on PSC 1b (STS) formation in the lower stratosphere (Blum et al., 2006; Achtert et al., 2011). PSC of type 1b are formed by the uptake of  $\text{HNO}_3$  on the liquid stratospheric background aerosol. The uptake by  $\text{H}_2\text{O}$  and  $\text{HNO}_3$  by the liquid aerosol particles is calculated by solving the growth and evaporation equation (Pruppacher and Klett, 1978) and using the parameterization of Luo et al. (1995) for the partial pressures of  $\text{H}_2\text{O}$  and  $\text{HNO}_3$ . Owing to the coupled uptake of  $\text{H}_2\text{O}$  and  $\text{HNO}_3$ , the  $\text{H}_2\text{SO}_4$  in the particles is considered as passive while the  $\text{H}_2\text{O}$  and  $\text{HNO}_3$  are considered as active components. The model is initialised with a particle ensemble consisting of pure  $\text{H}_2\text{SO}_4/\text{H}_2\text{O}$  aerosols and the  $\text{H}_2\text{O}$  in the aerosol particle is assumed to be always in equilibrium with the surrounding air. The considered particle ensemble is divided geometrically into  $N$  radial size bins and the aerosol number density in the size bins is calculated by using a log-normal distribution.

## 3 Observation and simulations

### 3.1 Arctic winter 2009/2010

The polar stratosphere was unusually cold during the Arctic winter 2009/2010, especially during the period between mid-December 2009 until end of January 2010. A comparison of ECMWF (European Centre of Medium-Range Weather Forecasts)

## Denitrification and polar stratospheric cloud formation

F. Khosrawi et al.

Title Page

Abstract

Introduction

Conclusions

References

Tables

Figures

◀

▶

◀

▶

Back

Close

Full Screen / Esc

Printer-friendly Version

Interactive Discussion





derived from Odin/SMR observations (Fig. 2). In this figure time series of  $\text{HNO}_3$  derived from Odin/SMR as well as time series of temperature derived from ECMWF analyses (averaged from profiles at the positions of the Odin/SMR measurements) are shown for potential temperature levels between 425 K and 625 K (between  $\approx 18$  and 30 km). The temperature time series show a decrease in temperature beginning in mid December. Toward the end of December the temperatures drop below the NAT formation temperature and with the formation of PSCs  $\text{HNO}_3$  is removed from the gas phase. Due to the continuous existence of PSCs between mid-December 2009 and end of January 2010  $\text{HNO}_3$  is further decreased. The occurrence of severe denitrification during the Arctic winter 2009/2010 at altitudes between 450 to 575 K (19 and 27 km) can be seen as the temperatures start to increase again after the major warming. The  $\text{HNO}_3$  mixing ratios do not reach the mixing ratios they had in mid-December 2009, before the PSC season started. The denitrification observed in January 2010 was also the strongest denitrification observed in the entire Odin measurement time period (2001–2010) (Fig. 3). Figure 3 shows the annual variability of  $\text{HNO}_3$  at potential temperature levels of 465–655 K for the Arctic winters 2001/2002 to 2009/2010 as derived from Odin/SMR observations as well as the UARS/MLS climatology derived for the years 1991–1998 (Santee et al., 2004). Very low  $\text{HNO}_3$  mixing ratios are found between 465 and 585 K ( $\approx 20$ –28 km) in mid of January that are even lower than in previous winters.

### 3.3 Lidar observations of PSC

Ground-based lidar measurements were performed with the IRF lidar in Kiruna and with the Esrangle lidar,  $\approx 25$  km east of Kiruna. Both lidar instruments perform measurements in two orthogonal polarisation directions so that the type of PSC can be derived from the measurements. The Esrangle lidar was operated from 16 January to 30 January 2010. During these 15 campaign days measurements were performed on 9 calendar days. A thick PSC layer was observed with a vertical extension of almost 10 km over a time period of 8 days. The composition of the observed PSCs was as follows: In the first three days of the measurement campaign the PSC was composed

## Denitrification and polar stratospheric cloud formation

F. Khosrawi et al.

Title Page

Abstract

Introduction

Conclusions

References

Tables

Figures



Back

Close

Full Screen / Esc

Printer-friendly Version

Interactive Discussion



---

**Denitrification and  
polar stratospheric  
cloud formation**

---

F. Khosrawi et al.

[Title Page](#)[Abstract](#)[Introduction](#)[Conclusions](#)[References](#)[Tables](#)[Figures](#)[⏪](#)[⏩](#)[◀](#)[▶](#)[Back](#)[Close](#)[Full Screen / Esc](#)[Printer-friendly Version](#)[Interactive Discussion](#)

of STS and NAT particles (17–20 January) and on 23 January, additionally, ice was observed. Thereby, the PSCs were mainly composed of STS with NAT layer at the bottom and/or top of the PSC and ice layers in between, respectively. On 23–24 January the PSC was composed of mainly NAT and some STS particles. After the major warming in mid-January only remnants of a PSC were found between 25 and 27 January. Measurements with the IRF lidar in Kiruna were performed between the 3 and 24 January. During this period measurements were performed during 15 calendar days. From 3–7 January the PSC was mainly composed of NAT. On 10 January an ice PSC was observed and after that the composition was a mixture between STS and mixed particles (STS and NAT). An overview of the measurements at Esrange and IRF are given in Tables 1 and 2.

### 3.4 Back trajectories and box model simulations

Back trajectories were calculated with the NOAA HYSPLIT (Hybrid Single Particle Lagrangian Integrated Trajectory Model) model based on GDAS (Global Data Assimilation System) analyses (<http://ready.arl.noaa.gov/HYSPLIT.php>). GDAS are meteorological analyses that are provided by the National Weather Service's National Centers for Environmental Prediction (NCEP). NCEP runs a series of computer analyses and forecasts operationally and one of the operational systems is GDAS. Analyses are provided four times a day (00:00, 06:00, 12:00 and 18:00 UTC). For each measurement performed with the Esrange and IRF lidar in January 2010, respectively, one to two trajectories (6-days backward) were calculated at three different altitudes. In general, a time has been chosen in the middle of the measurement or where the PSC was most pronounced during the measurement. A second time was chosen in case the PSC changed its composition or height extension during the measurement run. The three altitudes were chosen so that one trajectory is started at the bottom, one at the top and one in the middle of the observed PSC. An overview over the time, location and altitude where the trajectories have been started are given in Table 3.

**Denitrification and  
polar stratospheric  
cloud formation**

F. Khosrawi et al.

Title Page

Abstract

Introduction

Conclusions

References

Tables

Figures

◀

▶

◀

▶

Back

Close

Full Screen / Esc

Printer-friendly Version

Interactive Discussion



In total 63 trajectories were calculated. Box model simulations were performed for all trajectories simulating the uptake of  $\text{HNO}_3$  and  $\text{H}_2\text{O}$ , thus the formation of PSC type Ib (STS). Simulations of NAT or ice particles were not performed in this study since the nucleation processes for both particle types are still unclear. However, considering the temperature evolution along the trajectories we investigate which nucleation process for ice particle formation could have been possible. PSC type Ib formation is used to detect the PSC areas as well as the onset of PSC formation. NAT and ice particles are generally formed when temperatures drop below the ice formation temperature, thus after the onset of PSC type Ib formation. In the Arctic, NAT formation has generally been observed in connection with waves leading to a short, but sufficient temperature cooling (e.g., Voigt et al., 2000; Pagan et al., 2004). However, NAT formation has also been observed at temperatures above  $T_{\text{ice}}$  suggested heterogeneous formation of NAT on other particles than ice, as e.g. meteoric smoke particles (Voigt et al., 2005). Further, the box model simulation results are compared with the lidar measurements at Esrange and IRF which are located in the Kiruna area. During these measurements the PSCs were mostly composed of STS with only some layers of NAT or mixed particles in between.

The box model simulations were initialised with a log-normal distribution with a width of  $\sigma = 1.3$ , a total number density of  $n_{\text{tot}} = 8 \text{ cm}^{-3}$  and a mean radius of  $r_m = 0.062 \mu\text{m}$ , which is representative for the stratospheric background aerosol during Arctic winter as shown in earlier studies (Larsen et al., 2004; Blum et al., 2006; Achtert et al., 2011). The particle ensemble is divided geometrically into 26 size bins (B0–B25) with a volume ratio of 2, starting at a minimum particle radius of 30 nm (B0). Trace gas mixing ratios of  $\text{HNO}_3$ ,  $\text{H}_2\text{SO}_4$  and  $\text{H}_2\text{O}$  have been assumed as follows:  $\text{H}_2\text{SO}_4 = 0.5 \text{ pptv}$ ,  $\text{H}_2\text{O} = 5 \text{ ppmv}$  and  $\text{HNO}_3 = 8 \text{ ppbv}$ . These mixing ratios represent typical conditions in the polar winter stratosphere and are in agreement with Odin/SMR measurements. The ice existence temperature  $T_{\text{ice}}$  and the nitric acid trihydrate temperature  $T_{\text{NAT}}$  were calculated according to the parameterisations of Marti and Mauersberger (1993) and Hanson and Mauersberger (1988), respectively.

### 3.5 PSC observations by CALIPSO

PSCs were measured by CALIPSO during the Arctic winter 2009/2010. The measurements of PSCs by CALIPSO during that winter can be divided into four phases with distinctly different PSC optical characteristics (Pitts et al., 2011). The first phase (15–30 December 2009) was dominated by patchy, tenuous clouds consisting of liquid/NAT mixtures. The second phase (31 December 2009 to 14 January 2010) was characterized by the occurrence of mountain wave ice clouds along the east coast of Greenland, enhanced numbers of Mix-2 and Mix-2 enhanced particles as well as fully developed liquid STS clouds. The third distinct phase occurred from 15 to 21 January 2010 when temperatures synoptically cooled below  $T_{ice}$  resulting in synoptic-scale ice PSCs. The cold pool was located in the area north of Scandinavia, between Svalbard and Novaya Zemlya. Further, during this time period the numbers of Mix-1, Mix-2 and Mix-2 enhanced particles decreased significantly compared with the previous periods. The presence of widespread ice PSCs disappeared abruptly after the 21 January when after the major warming temperatures increased above  $T_{ice}$ . The fourth and last phase occurred from 22 to 28 January 2010 was dominated by liquid STS clouds. A detailed description and examples of the PSCs observed by CALIPSO during the Arctic winter 2009/2010 can be found in Pitts et al. (2011).

## 4 Results

### 4.1 Trajectories and box model simulations

The backward trajectories were calculated starting from IRF Kiruna and from Esrangle, respectively, at times and dates when PSCs were measured. During the course of the 6-days the trajectories in general followed the circular flow within the polar vortex and thus the air masses were transported once around in the polar regions. Figure 4 shows the three trajectories that were calculated with HYSPLIT for the lidar measurement at

## Denitrification and polar stratospheric cloud formation

F. Khosrawi et al.

Title Page

Abstract

Introduction

Conclusions

References

Tables

Figures



Back

Close

Full Screen / Esc

Printer-friendly Version

Interactive Discussion



## Denitrification and polar stratospheric cloud formation

F. Khosrawi et al.

Title Page

Abstract

Introduction

Conclusions

References

Tables

Figures

◀

▶

◀

▶

Back

Close

Full Screen / Esc

Printer-friendly Version

Interactive Discussion



Esrangle on 23 January 2010 at 19:00 UTC. Although at all three altitudes (19, 22 and 25 km) the air masses were transported over Russia and the Arctic sea to the Esrange, the air masses at these altitudes had different origin. The air mass at 19 km was originating from Russia, while the air mass at 22 km was originating from the sea north of Scandinavia, between Svalbard and Novaya Zemlya and the air mass at 25 km originated from Greenland. From Fig. 4 it can be seen that the air mass at 25 km was transported furthest during the 6-days compared to the air masses at 19 and 22 km. Though the trajectories have a different origin, the trajectories started at 22 and 25 km passed the area around Scandinavia twice, once the area was passed around Kiruna and once around the area somewhat north of Scandinavia.

The temperatures along the trajectories were generally for several hours below  $T_{\text{NAT}}$ , and occasionally also reached below  $T_{\text{ice}}$  (this usually happened 5 to 6-days before the measurements were performed). Temperatures below  $T_{\text{ice}}$  were found north of Scandinavia, over the sea between Svalbard and Novaya Zemlya. The box model simulations show that PSCs are generally simulated at the begin (time of the lidar measurements) and occasionally at the end (5 to 6-days before the lidar measurements) of the trajectories when trajectories passed through the cold pool between Scandinavia, Svalbard and Novaya Zemlya. Thus the simulation results can be divided into two parts, PSC formation in the Kiruna area and PSC formation in the area north of Scandinavia.

### 4.2 PSC formation in the area of Kiruna

Figure 5 shows one of the microphysical box model simulations where PSC formation was simulated at the begin and end of the trajectory. This simulation was performed at 23 January starting at Esrange at 19:00 UT at 22 km (the green trajectory in Fig. 4). The simulation starts at the end of the trajectory, thus at the location and time from where the air mass originated since the box model simulation is performed forward in time while the trajectories are calculated backward in time. Thus, the end of the simulation (from  $t = -30$  h onwards) shows the PSC formation in the area of Kiruna. At  $t = -30$  h  $T_{\text{NAT}}$  is reached and the liquid  $\text{H}_2\text{SO}_4/\text{H}_2\text{O}$  particles start to take up  $\text{HNO}_3$ . As the

## Denitrification and polar stratospheric cloud formation

F. Khosrawi et al.

Title Page

Abstract

Introduction

Conclusions

References

Tables

Figures

◀

▶

◀

▶

Back

Close

Full Screen / Esc

Printer-friendly Version

Interactive Discussion



temperature decreases further (almost reaching  $T_{ice}$ ) more and more  $HNO_3$  is taken up and with a weight percentage of 40%  $HNO_3$  fully developed STS PSCs are formed. The simulation of a STS PSC at 22 km is in agreement with the lidar measurements with the Esrange lidar at this altitude as can be seen from Fig. 6. The figure shows the lidar measurement of backscatter in parallel and perpendicular polarisation on 23 January at 19:00 UTC. A PSC that extended over the altitude range from 17.5 to 25.5 km was measured. The PSC consisted of two layers with maxima in parallel and perpendicular backscatter ratio at 20 and 24 km. The composition was mainly STS with some NAT and mixed layers at the bottom and top of the PSC. The simulations at 19 km and 25 km (not shown) are also in agreement with the lidar measurement at these altitudes.

PSC occurrence in the Kiruna area was dominated by NAT in the begin of January (3–7 January) and dominated by STS clouds (with some NAT and mixed layers in between as in Fig. 6) from mid January to end of January (11–20 January). Temperatures were generally for several hours below  $T_{NAT}$  but never reached  $T_{ice}$ . Uptake of  $HNO_3$  by the liquid  $H_2SO_4/H_2O$  aerosols and PSC type Ib formation occurred 10 h (17 January) and 40 h (24 January), respectively, before the lidar measurements were performed (Fig. 5). This indicates in agreement with the measurements that during that time period the same PSC persisted over Kiruna with differing strength. The PSC was most pronounced in the microphysical box model simulation between 22 and 24 January which also is in agreement with the lidar measurements performed in Kiruna.

### 4.3 PSC formation north of Scandinavia

For investigating PSCs that were simulated north of Scandinavia we have to focus on the time between  $t = -140$  h and  $t = -110$  h, thus at the begin of the box model simulation (Fig. 5). As the air mass passes over the sea between Scandinavia and Svalbard temperatures reach below  $T_{ice}$  for approximately 15 h (Figs. 4 and 5). Due to these cold temperatures  $HNO_3$  is taken up and STS PSCs are formed. However, due to these low temperatures also formation of NAT and ice PSCs is possible which are not included in this simulation but will be discussed later based on measurements.

**Denitrification and  
polar stratospheric  
cloud formation**

F. Khosrawi et al.

Title Page

Abstract

Introduction

Conclusions

References

Tables

Figures

◀

▶

◀

▶

Back

Close

Full Screen / Esc

Printer-friendly Version

Interactive Discussion



The occurrence of temperatures below  $T_{ice}$  show that the air masses were originating from the regions where the center of the vortex with the coldest temperatures was located (north of Scandinavia). The temperatures along the trajectories were for several hours below  $T_{NAT}$  and reached also for some hours below  $T_{ice}$ . PSC formation was simulated generally 130 to 90 h before the lidar measurements were performed. The PSC were most pronounced along the trajectories started between 22 and 24 January (thus these show the PSC that occurred between 14 to 18 January north of Scandinavia). Since ground-based lidar measurements are not available at the locations where the trajectories originate we compare these simulations with space-borne measurements from CALIPSO.

Figure 7 shows the CALIPSO composition observation on 18 January at 00:19 UTC. The CALIPSO track passes from east of Scandinavia northwards crossing the trajectory that was calculated on 23 January 6-days backward, thus crossing the trajectory approximately on 18 January. On that overpass CALIPSO observed a PSC that extended from 17 to 20 km up to 25 to 26 km (depending on latitude and longitude). The PSC was composed of STS, Mix 1, Mix 2 as well as ice particles which coincides with the temperatures below  $T_{ice}$  as found along the trajectories. Thus, though we do not explicitly calculate NAT and ice we know from the temperature history of the trajectory and the CALIPSO measurements that in that area all three PSC types were present at the same time. Further, this shows that the temperature history derived from HYSPLIT based on NCEP analyses and the CALIPSO measurements are in agreement. The ice PSCs during that time period were caused by a synoptic-scale cooling of the air mass as was discussed in Pitts et al. (2011).

#### 4.4 PSC formation and denitrification

To investigate where exactly the cold temperatures generally occurred during the Arctic winter 2009/2010 and thus if these areas agree with the areas where ice PSCs and denitrification was observed, the coordinates where temperatures below  $T_{ice}$  were encountered along the trajectories are plotted on a map (Fig. 8). Thereby, the trajectories

started at Esrange as well as the trajectories started from IRF Kiruna are included. This figure shows that temperatures below  $T_{ice}$  were reached above the sea west of Greenland on 2 January and at several locations northeast of Scandinavia (between Svalbard and Novaya Zemlya) on the 15, 17 and 18 January. While the temperatures below  $T_{ice}$  were caused by waves on 2 January they were caused by a synoptic-scale cooling for 15–18 January.

To compare the areas where  $T_{ice}$  was encountered along the trajectories with the locations where ice PSCs were observed by CALIPSO these locations were also included in this figure. Note: only one coordinate pair (lat/lon) per ice PSC has been chosen (center of the cloud). The PSC measured by CALIPSO agree well with the regions where  $T_{ice}$  was found along the trajectories. Further, the PSC formation north of Scandinavia agrees spatially and locally quite well with the area where denitrification was observed by Odin/SMR (compare Fig. 8 with Fig. 1). Thus, from this coincidence we suggest that ice formation on NAT particles with subsequent sedimentation of these particles caused the denitrification as observed by Odin/SMR. Pitts et al. (2011) found an increase in ice PSC observations with a coincident decrease in NAT mixture observations indicating that heterogeneous nucleation on NAT particles may be an important mechanism for the formation of synoptic-scale ice PSCs and thus their findings are in agreement with our findings. Further, our finding and the finding by Pitts et al. (2011) are corroborated by balloon measurements of  $H_2O$  made in Sodankylä (67.3° N, 26.4° E) showing dehydration. If denitrification was caused by sedimenting ice particles concurrent dehydration must occur. Trajectory analyses according to the balloon measurements made in Sodankylä showed that the air masses were dehydrated during 16 to 19 January and that the dehydrated air was originating from the area north of Scandinavia where the cold temperatures were observed (Sergey Khaykin, personal communication, 2011).

**Denitrification and  
polar stratospheric  
cloud formation**

F. Khosrawi et al.

Title Page

Abstract

Introduction

Conclusions

References

Tables

Figures

◀

▶

◀

▶

Back

Close

Full Screen / Esc

Printer-friendly Version

Interactive Discussion



## 5 Conclusions

Denitrification was observed by Odin/SMR during the Arctic winter 2009/2010. A comparison of the Odin/SMR measurements for the last ten years shows that this was the strongest denitrification event in the entire Odin/SMR measuring period (2001–2010).

Here, we use a combination of ground-based and space-borne lidar measurements together with microphysical box model simulations to investigate PSC formation and denitrification during the Arctic winter 2009/2010. Ground-based lidar measurements were performed in the area of Kiruna at IRF (67.8° N, 20.4° E) from 3 to 24 January and from 16 to 30 January at Esrange (67.8° N, 21.1° E), respectively. In the Kiruna area the PSC were dominated by NAT in the beginning of January and the by STS with some mixed or NAT layers at the bottom and/or top of the PSC. A distinct ice cloud was solely observed once, namely on 10 January by the IRF lidar in Kiruna.

Trajectories were calculated with HYSPLIT based on the NCEP/GDAS meteorological analyses. The temperatures along the trajectories reached generally below  $T_{\text{NAT}}$  for several hours but temperatures below  $T_{\text{ice}}$  were only encountered occasionally when the air mass was transported over the areas north of Scandinavia, over the sea between Svalbard and Novaya Zemlya. In this region the center of the vortex was located that cooled down synoptically during the course of the winter to temperatures below  $T_{\text{ice}}$  (15–21 January). Microphysical box model simulations along the HYSPLIT trajectories simulating STS cloud formation show that in case when the air mass passed the cold pool that PSC formation of PSCs type Ib can be simulated in the Kiruna area as well as North of Scandinavia. Due to the extremely low temperatures encountered north of Scandinavia, besides STS formation NAT and ice formation that has not been considered in the simulations can be expected in this area. In fact, NAT and ice PSCs were observed by CALIPSO in mid January north of Scandinavia.

Comparison of the area where the trajectories encounter temperatures below  $T_{\text{ice}}$  and measurements of ice PSCs by CALIPSO show that these areas are in good agreement. Further, this area is also collocated with the area where denitrification

### Denitrification and polar stratospheric cloud formation

F. Khosrawi et al.

Title Page

Abstract

Introduction

Conclusions

References

Tables

Figures

◀

▶

◀

▶

Back

Close

Full Screen / Esc

Printer-friendly Version

Interactive Discussion



by Odin/SMR was observed. Thus, this consistency suggest that during this particular winter denitrification could have been caused by sedimenting ice particles that had formed on NAT particles. A denitrification caused by sedimenting ice particles occurs in general with a concurrant dehydration. Dehydration was observed in ballon measurements made from Sodankylä (67.3° N, 26.4° E). Trajectory analyses showed that the air masses were dehydrated between 16 and 19 January and that the dehydrated air was originating from the area north of Scandinavia where the cold temperatures were observed (Sergey Khaykin, personal communication, 2011). Further, our results are in agreement with Pitts et al. (2011) who found an increase in ice PSC observations and coincident decrease in NAT mixture observations and suggested that this indicates heterogeneous nucleation of ice on NAT particles may be an important mechanism for the formation of synoptic-scale ice PSCs.

*Acknowledgements.* We are grateful to the European Space Agency (ESA) for providing the Odin/SMR data. Odin is a Swedish led project funded jointly by Sweden (SNSB), Canada (CSA), Finland (TEKES), and France (CNES) and the European Space Agency (ESA). The authors gratefully acknowledge the NOAA Air Resources Laboratory (ARL) for the provision of the HYSPLIT transport and dispersion model and/or READY website (<http://www.arl.noaa.gov/ready.php>) used in this publication. We would like to thank P. Konopka for the diffusive uptake code and P. Deuflhard and U. Nowak for providing the solver for ordinary differential equations used in the microphysical box model. Further, we would like to thank U. Blum for help with PSC classification and analyses of lidar data and R. Müller for helpful discussions. We are also grateful to the Swedish Research Council for funding F. Khosrawi.

## References

- Achtert, P., Khosrawi, F., Blum, U., and Fricke, K.-H.: Investigation of polarstratospheric clouds in January 2008 by means of ground-based and space-borne lidar measurements and microphysical box model simualations, *J. Geophys. Res.*, 116, D07201, doi:10.1029/2010JD014803, 2011. 11387, 11391
- Biermann, U. M., Crowley, J. N., Huthwelker, T., Moortgat, G. K., Crutzen, P. J., and Peter, T.:

## Denitrification and polar stratospheric cloud formation

F. Khosrawi et al.

Title Page

Abstract

Introduction

Conclusions

References

Tables

Figures



Back

Close

Full Screen / Esc

Printer-friendly Version

Interactive Discussion



**Denitrification and  
polar stratospheric  
cloud formation**

F. Khosrawi et al.

Title Page

Abstract

Introduction

Conclusions

References

Tables

Figures

◀

▶

◀

▶

Back

Close

Full Screen / Esc

Printer-friendly Version

Interactive Discussion



FTIR studies on lifetime prolongation of stratospheric ice particles due to NAT coating, *Geophys. Res. Lett.*, 21, 3939–3942, doi:10.1029/1998GL900040, 1998. 11382

Blum, U. and Fricke, K. H.: The Bonn University lidar at the Esrange: technical description and capabilities for atmospheric research, *Ann. Geophys.*, 23, 1645–1658, doi:10.5194/angeo-23-1645-2005, 2005. 11386

Blum, U., Fricke, K. H., Müller, K. P., Siebert, J., and Baumgarten, G.: Long-term lidar observations of polar stratospheric clouds at Esrange in Northern Sweden, *Tellus B*, 57, 412–422, 2005. 11386

Blum, U., Khosrawi, F., Baumgarten, G., Stebel, K., Müller, R., and Fricke, K. H.: Simultaneous lidar observations of a polar stratospheric cloud on the east and west sides of the Scandinavian mountains and microphysical box model simulations, *Ann. Geophys.*, 24, 3267–3277, doi:10.5194/angeo-24-3267-2006, 2006. 11386, 11387, 11391

Browell, E. V., Butler, C. F., Ismail, S., Robinette, P. A., Carter, A. F., Higdon, N. S., Toon, O. B., Schoeberl, M., and Tuck, A. F.: Airborne LIDAR observations in the wintertime Arctic stratosphere: polar stratospheric clouds, *Geophys. Res. Lett.*, 17, 385–388, 1990. 11381, 11386

Carslaw, K. S., Luo, B. P., Clegg, S. L., Peter, T., Brimblecombe, P., and Crutzen, P. J.: Stratospheric aerosol growth and HNO<sub>3</sub> gas phase depletion from coupled HNO<sub>3</sub> and water uptake by liquid particles, *Geophys. Res. Lett.*, 21, 2479–2482, 1994. 11381

Crutzen, P. J. and Arnold, F.: Nitric acid cloud formation in the cold Antarctic stratosphere: a major cause for the springtime “ozone hole”, *Nature*, 342, 651–655, 1986. 11381

Dörnbrack, A., Pitts, M. C., and Poole, L. R.: The winter Arctic stratosphere in 2009/2010 – overview, gravity wave activity and predictability of sudden stratospheric warmings, *Atmos. Chem. Phys. Discuss.*, 11, in preparation, 2011. 11388

Drdla, K. and Browell, E. V.: Microphysical modeling of the 1999–2000 Arctic winter: 3. impact of homogeneous freezing on polar stratospheric clouds, *J. Geophys. Res.*, 109, D10201, doi:10.1029/2003JD004352, 2004. 11381

Drdla, K. and Turco, R. P.: A 1-D model incorporating temperature oscillations, *J. Atmos. Chem.*, 12, 319–366, 1991. 11382

Fahey, D. W., Kelly, K. K., Kawa, S. R., Tuck, A. F., Loewenstein, M., Chan, K. R., and Heid, L. E.: Observations of denitrification and dehydration in the winter polar stratosphere, *Nature*, 344, 321–324, 1990. 11383

Fahey, D. W., Gao, R. S., Carslaw, K. S., Kettleborough, J., Popp, P. J., Northway, M. J., Holecek, J. C., Ciciora, S. C., McLaughlin, R. J., Thompson, T. L., Winkler, R. H., Baumgard-

## Denitrification and polar stratospheric cloud formation

F. Khosrawi et al.

Title Page

Abstract

Introduction

Conclusions

References

Tables

Figures

◀

▶

◀

▶

Back

Close

Full Screen / Esc

Printer-friendly Version

Interactive Discussion



ner, D. G., Gandrud, B., Wennberg, P. O., Dhaniyala, S., McKinley, K., Peter, T., Salawitch, R. J., Bui, T. P., Elkins, J. W., Webster, C. R., Atlas, E. L., Jost, H., Wilson, J. C., Herman, R. L., Kleinböhl, A., and von König, M.: The detection of large HNO<sub>3</sub>-containing particles in the winter Arctic stratosphere, *Science*, 291, 1026–1031, 2001. 11382, 11383

5 Hanson, D. R. and Mauersberger, K.: Laboratory studies of the nitric acid trihydrate: implications for the south polar stratosphere, *Geophys. Res. Lett.*, 15, 855–858, 1988. 11381, 11391

Khosrawi, F. and Konopka, P.: Enhancement of nucleation and condensation rates due to mixing processes in the tropopause region, *Atmos. Environ.*, 37, 903–910, 2003. 11387

10 Khosrawi, F., Ström, J., Minikin, A., and Krejci, R.: Particle formation in the Arctic free troposphere during the ASTAR 2004 campaign: a case study on the influence of vertical motion on the binary homogeneous nucleation of H<sub>2</sub>SO<sub>4</sub>/H<sub>2</sub>O, *Atmos. Chem. Phys.*, 10, 1105–1120, doi:10.5194/acp-10-1105-2010, 2010. 11387

Knopf, D. A., Koop, T., Luo, B. P., Weers, U. G., and Peter, T.: Homogeneous nucleation of NAD and NAT in liquid stratospheric aerosols: insufficient to explain denitrification, *Atmos. Chem. Phys.*, 2, 207–214, doi:10.5194/acp-2-207-2002, 2002. 11382

Koop, T., Biermann, U. M., Raber, W., Luo, B. P., Crutzen, P. J., and Peter, T.: Do stratospheric aerosol droplets freeze above the ice frost point?, *Geophys. Res. Lett.*, 22, 917–920, 1995. 11381, 11382

20 Koop, T., Carslaw, K. S., and Peter, T.: Thermodynamic stability and phase transitions of PSC particles, *Geophys. Res. Lett.*, 24, 2199–2202, 1997. 11382

Koop, T., Luo, B., Tsias, A., and Peter, T.: Water activity as the determinant for homogeneous ice nucleation in aqueous solutions, *Nature*, 406, 611–614, 2000. 11382

25 Larsen, N., Knudsen, B. M., Rosen, J. M., Kjöme, N. T., Neuber, R., and Kyrö, E.: Temperature histories in liquid and solid polar stratospheric cloud formation, *J. Geophys. Res.*, 102, 23505–23517, 1997. 11381, 11382

Larsen, N., Hoyer Svendsen, S., Knudsen, B. M., Mikkelsen, I. S., Voigt, C., Kohlmann, A., Schreiner, J., Mauersberger, K., Deshler, T., Kröger, C., Rosen, J. M., Kjöme, N. T., Adriani, A., Cairo, F., Di Donfrancesco, G., Ovarlez, J., Ovarlez, H., Dörnbrack, A., and Birner, T.: Microphysical mesoscale simulation of polar stratospheric cloud formation constrained by in situ measurements of chemical and optical cloud properties, *J. Geophys. Res.*, 107, 8301, doi:10.1029/2001JD000999, 2002. 11381, 11382, 11383

Larsen, N., Knudsen, B. M., Svendsen, S. H., Deshler, T., Rosen, J. M., Kivi, R., Weisser, C.,

**Denitrification and  
polar stratospheric  
cloud formation**

F. Khosrawi et al.

Title Page

Abstract

Introduction

Conclusions

References

Tables

Figures

◀

▶

◀

▶

Back

Close

Full Screen / Esc

Printer-friendly Version

Interactive Discussion



Schreiner, J., Mauerberger, K., Cairo, F., Ovarlez, J., Oelhaf, H., and Spang, R.: Formation of solid particles in synoptic-scale Arctic PSCs in early winter 2002/2003, *Atmos. Chem. Phys.*, 4, 2001–2013, doi:10.5194/acp-4-2001-2004, 2004. 11391

Lowe, D. and MacKenzie, R.: Review: Polar stratospheric cloud microphysics and chemistry, *J. Atmos. Sol.-Terr. Phys.*, 70, 13–40, 2008. 11381

Luo, B., Carslaw, K. S., Peter, T., and Clegg, S. L.: Vapour pressures of  $\text{H}_2\text{SO}_4/\text{HNO}_3/\text{HCl}/\text{HBr}/\text{H}_2\text{O}$  solutions to low stratospheric temperatures, *Geophys. Res. Lett.*, 22, 247–250, 1995. 11387

Marti, J. and Mauersberger, K.: A survey and new measurements of ice vapor pressure temperatures between 170 and 250 K, *Geophys. Res. Lett.*, 20, 363–366, 1993. 11391

McCormick, M. P., Steele, H. M., Hamill, P., Chu, W. P., and Swissler, T.: Polar stratospheric cloud sightings by SAM II, *J. Atmos. Sci.*, 39, 1387–1397, 1982. 11381

Meilinger, S., Koop, K., Luo, B. P., Huthwelker, T., Carslaw, K. S., Krieger, U., Crutzen, P. J., and Peter, T.: Size-dependent stratospheric droplet composition in lee wave temperature fluctuations and their potential role in PSC freezing, *Geophys. Res. Lett.*, 22, 3031–3034, 1995. 11381

Murtagh, D., Frisk, U., Merino, F., Ridal, M., Jonsson, A., Stegman, J., Witt, G., Eriksson, P., Jimenez, C., Megie, G., de la Noe, J., Ricaud, P., Baron, P., Pardo, J. R., Hauchcorne, A., Llewellyn, E. J., Degenstein, D. A., Gattinger, R. L., Lloyd, N. D., Evans, W. F. J., McDade, I. C., Haley, C. S., Sioris, C., von Savigny, C., Solheim, B. H., McConnell, J. C., Strong, K., Richardson, E. H., Leppelmeier, G. W., Kyrola, E., Auvinen, H., and Oikarinen, L.: An overview of the Odin atmospheric mission, *Can. J. Phys.*, 80, 309–319, 2002. 11384

Ovarlez, J. O. and Ovarlez, H.: Stratospheric water vapor content evolution during EASOE, *Geophys. Res. Lett.*, 21, 1235–1238, 1994. 11383

Pagan, K. L., Tabazadeh, A., Drdla, K., Hervig, M., Eckermann, S. D., Browell, E. V., Legg, M. L., and Froschi, P. G.: Observational evidence against mountain wave-wave generation of ice nuclei as prerequisite for the formation of three solid nitric acid polar stratospheric clouds observed in the Arctic in early December 1999, *J. Geophys. Res.*, 109, D04312, doi:10.1029/2003JD003846, 2004. 11391

Pawson, S., Naujokat, B., and Labitzke, K.: On the polar stratospheric cloud formation potential on the northern stratosphere, *J. Geophys. Res.*, 104, 14209–14222, 1995. 11388

Peter, T.: Microphysics and heterogeneous chemistry of polar stratospheric clouds, *Annu. Rev. Phys. Chem.*, 48, 785–822, 1997. 11381, 11382

**Denitrification and  
polar stratospheric  
cloud formation**

F. Khosrawi et al.

Title Page

Abstract

Introduction

Conclusions

References

Tables

Figures

◀

▶

◀

▶

Back

Close

Full Screen / Esc

Printer-friendly Version

Interactive Discussion



- Pitts, M. C., Thomason, L. W., Poole, L. R., and Winker, D. M.: Characterization of Polar Stratospheric Clouds with spaceborne lidar: CALIPSO and the 2006 Antarctic season, *Atmos. Chem. Phys.*, 7, 5207–5228, doi:10.5194/acp-7-5207-2007, 2007. 11385
- Pitts, M. C., Poole, L. R., and Thomason, L. W.: CALIPSO polar stratospheric cloud observations: second-generation detection algorithm and composition discrimination, *Atmos. Chem. Phys.*, 9, 7577–7589, doi:10.5194/acp-9-7577-2009, 2009. 11385
- Pitts, M. C., Poole, L. R., Dörnbrack, A., and Thomason, L. W.: The 2009–2010 Arctic polar stratospheric cloud season: a CALIPSO perspective, *Atmos. Chem. Phys.*, 11, 2161–2177, doi:10.5194/acp-11-2161-2011, 2011. 11382, 11383, 11385, 11388, 11392, 11395, 11396, 11398
- Poole, L. R. and McCormick, M. P.: Polar stratospheric clouds and the Antarctic ozone hole, *J. Geophys. Res.*, 93, 8423–8430, 1988. 11381
- Pruppacher, H. and Klett, J. D.: *Microphysics of Clouds and Precipitation*, D. Reidel, Norwell, MS, 1978. 11387
- Salcedo, D., Molina, L. T., and Molina, M. J.: Homogeneous freezing of concentrated aqueous nitric acid solutions at polar stratospheric temperatures, *J. Phys. Chem.*, 105, 1433–1439, 2001. 11382
- Santee, M., Manney, G., Livesey, N., and Read, W.: Three-dimensional structure and evolution of HNO<sub>3</sub> based on UARS Microwave Limb Sounder measurements, *J. Geophys. Res.*, 109, D15206, doi:10.1029/2004JD004578, 2004. 11389
- Solomon, S.: Stratospheric ozone depletion: a review of concepts and history, *Rev. Geophys.*, 37, 275–316, 1999. 11381
- Solomon, S., Garcia, R. R., Rowland, F. S., and Wuebbles, D. J.: On the depletion of Antarctic ozone, *Nature*, 321, 755–758, 1986. 11381
- Steele, H. M., Hamill, P., McCormick, M. P., and Swissler, T. J.: The formation of polar stratospheric clouds, *J. Atmos. Sci.*, 40, 2055–2067, 1983. 11381
- Tabazadeh, A., Toon, O. B., and Hamill, P.: Freezing behaviour of stratospheric sulfate aerosols inferred from trajectory studies, *Geophys. Res. Lett.*, 22, 1725–1728, 1995. 11381
- Tabazadeh, A., Toon, O. B., Gary, B. L., Bacmeister, J. T., and Schoeberl, M. R.: Observational constraints on the formation of type 1a polar stratospheric clouds, *Geophys. Res. Lett.*, 23, 2109–2112, 1996. 11382
- Toon, O. B., Hamill, P., Turco, R. P., and Pinto, J.: Condensation of HNO<sub>3</sub> and HCl in winter polar stratospheres, *Geophys. Res. Lett.*, 13, 1284–1287, 1986. 11381

## Denitrification and polar stratospheric cloud formation

F. Khosrawi et al.

Title Page

Abstract

Introduction

Conclusions

References

Tables

Figures

◀

▶

◀

▶

Back

Close

Full Screen / Esc

Printer-friendly Version

Interactive Discussion



Toon, O. B., Tabazadeh, A., and Browell, E. V.: Analyses of lidar observations of Arctic polar stratospheric clouds during January 1989, *J. Geophys. Res.*, 105, 20589–20615, 2000. 11381, 11382

Urban, J., Lautié, N., Le Flochmoën, E., Jiménez, C., Eriksson, P., De La Noë, J., Dupuy, E., Ekström, M., El Amraoui, L., Frisk, U., Murtagh, D., Olberg, M., and Ricaud, P.: Odin/SMR limb observations of stratospheric trace gases: level 2 processing of ClO, N<sub>2</sub>O, HNO<sub>3</sub>, and O<sub>3</sub>, *J. Geophys. Res.*, 110, D14307, doi:10.1029/2005JD005741, 2005. 11384

Urban, J., Murtagh, D., Lautié, N., Barret, B., Dupuy, E., De La Noë, J., Eriksson, P., Frisk, U., Jones, A., Le Flochmoën, E., Olberg, M., Piccolo, C., Ricaud, P., and Rösevall, J.: Odin/SMR limb observations of trace gases in the polar lower stratosphere during 2004–2005, in: Proceedings of the ESA First Atmospheric Science Conference, 8–12 May 2006, Frascati, Italy, edited by: H. Lacoste, Eur. Space Agency Spec. Publ., 2006. 11385

Urban, J., Pommier, M., Murtagh, D. P., Santee, M. L., and Orsolini, Y. J.: Nitric acid in the stratosphere based on Odin observations from 2001 to 2009 – Part 1: A global climatology, *Atmos. Chem. Phys.*, 9, 7031–7044, doi:10.5194/acp-9-7031-2009, 2009. 11384, 11385

Voigt, C., Schreiner, J., Kohlmann, A., Zink, P., Mauersberger, K., Larsen, N., Deshler, T., Kröger, C., Rosen, J., Adriani, A., Cairo, F., Donfrancesco, G. D., Viterbini, M., Ovarlez, J., Ovarlez, H., David, C., and Dörnbrack, A.: Nitric acid trihydrate (NAT) in polar stratospheric clouds, *Science*, 290, 1756–1758, 2000. 11382, 11391

Voigt, C., Schlager, H., Luo, B. P., Dörnbrack, A., Roiger, A., Stock, P., Curtius, J., Vössing, H., Borrmann, S., Davies, S., Konopka, P., Schiller, C., Shur, G., and Peter, T.: Nitric Acid Trihydrate (NAT) formation at low NAT supersaturation in Polar Stratospheric Clouds (PSCs), *Atmos. Chem. Phys.*, 5, 1371–1380, doi:10.5194/acp-5-1371-2005, 2005. 11382, 11391

Vömel, H., Rummukainen, M., Kivi, R., Karhu, J., Turunen, T., Kyrö, E., Rosen, J., Kjome, N., and Oltmans, S.: Dehydration and sedimentation of ice particles in the Arctic stratospheric vortex, *Geophys. Res. Lett.*, 24, 798–798, 1997. 11383

von Hobe, M., Grooss, J. U., Pope, F., Peter, T., Cairo, F., Orsolini, Y., Volk, C. M., Marchand, D. M., Janosi, I. M., Schlager, H., Stroh, F., Rex, M., Wienhold, F., et al.: Reconciliation of essential process parameters for an enhanced predictability of Arctic stratospheric ozone loss and its climate interactions, *Atmos. Chem. Phys. Discuss.*, 11, in preparation, 2011. 11384

Winker, D. M., Hunt, W. H., and McGill, M.: Initial performance assessment of CALIOP, *Geophys. Res. Lett.*, 34, L19803, doi:10.1029/2007GL030135, 2007. 11385

Zondlo, M. A., Hudson, P. K., Prenni, A. J., and Tolbert, M. A.: Chemistry and microphysics of polar stratospheric clouds and cirrus clouds, *Annu. Rev. Phys. Chem.*, 51, 473–499, 2000. 11382

---

**Denitrification and polar stratospheric cloud formation**

F. Khosrawi et al.

---

Title Page

Abstract

Introduction

Conclusions

References

Tables

Figures



Back

Close

Full Screen / Esc

Printer-friendly Version

Interactive Discussion



## Denitrification and polar stratospheric cloud formation

F. Khosrawi et al.

**Table 1.** PSC observations with the Esrange lidar during the campaign period 16 to 30 January 2010.

Start Date/Time	End Date/Time	PSC observations
17 Jan 12:14 UT	17 Jan 17:42 UT	PSC at 19–26 km (STS)
19 Jan 17:32 UT	19 Jan 01:30 UT	PSC at 19–26 km (STS and NAT)
20 Jan 12:45 UT	20 Jan 14:24 UT	PSC at 20–25 km (STS and NAT)
22 Jan 01:01 UT	22 Jan 05:40 UT	weak PSC (STS)
22 Jan 17:02 UT	23 Jan 12:19 UT	PSC at 16.5–26.5 km (STS, NAT and ice needles)
23 Jan 12:26 UT	24 Jan 03:24 UT	PSC at 17.5–26.5 km (NAT dominated with STS)
24 Jan 13:23 UT	24 Jan 18:20 UT	PSC at 17–25 km (Mixed and STS)
25 Jan 21:41 UT	26 Jan 00:23 UT	no PSC
28 Jan 17:30 UT	28 Jan 18:50 UT	remnants of a PSC at 18–25 km
30 Jan 18:10 UT	30 Jan 20:16 UT	traces of a PSC

Title Page

Abstract

Introduction

Conclusions

References

Tables

Figures

◀

▶

◀

▶

Back

Close

Full Screen / Esc

Printer-friendly Version

Interactive Discussion



## Denitrification and polar stratospheric cloud formation

F. Khosrawi et al.

Title Page

Abstract

Introduction

Conclusions

References

Tables

Figures

⏪

⏩

◀

▶

Back

Close

Full Screen / Esc

Printer-friendly Version

Interactive Discussion



**Table 2.** PSC observations with the IRF lidar during January 2010.

Start Date/Time	End Date/Time	PSC observation
3 Jan 16:45 UT	3 Jan 18:50 UT	17–24 km (NAT)
4 Jan 13:35 UT	4 Jan 19:50 UT	18–24 km (NAT)
6 Jan 13:55 UT	6 Jan 23:50 UT	19–26 km (NAT)
7 Jan 20:10 UT	8 Jan 02:30 UT	18–25 km (NAT)
10 Jan 15:55 UT	11 Jan 02:30 UT	26+ km (Ice)
11 Jan 17:05 UT	11 Jan 22:40 UT	23–24 km (STS, Mix)
12 Jan 20:49 UT	13 Jan 04:00 UT	21–24 km (STS, Mix)
14 Jan 15:05 UT	15 Jan 05:15 UT	20–27 km (STS, Mix)
15 Jan 15:00 UT	16 Jan 07:30 UT	20–25 km (STS, Mix)
16 Jan 21:10 UT	17 Jan 05:00 UT	20–26 km (STS, Mix)
17 Jan 21:20 UT	17 Jan 23:00 UT	19–25 km (STS, Mix)
19 Jan 16:35 UT	20 Jan 00:45 UT	21–24 km (STS, Mix)
22 Jan 04:30 UT	22 Jan 07:20 UT	18–25 km (STS, Mix)
22 Jan 15:15 UT	23 Jan 06:15 UT	18–25 km (STS, Mix)
23 Jan 15:35 UT	24 Jan 01:55 UT	18–25 km (STS, Mix)
24 Jan 17:05 UT	24 Jan 20:25 UT	17–22 km (STS, Mix)

## Denitrification and polar stratospheric cloud formation

F. Khosrawi et al.

Title Page

Abstract

Introduction

Conclusions

References

Tables

Figures

◀

▶

◀

▶

Back

Close

Full Screen / Esc

Printer-friendly Version

Interactive Discussion



**Table 3.** Starting dates and times of the trajectories calculated with HYSPLIT. The starting dates and times haven been chosen based on the measurements with the Esrange and IRF lidar.

Start Date/Time	Start Location	Start Lat/Lon	Altitudes
19 Jan 22:00 UT	Esrange	67.8° N/21.1° E	22, 23, 25 km
20 Jan 14:00 UT	Esrange	67.8° N/21.1° E	21, 23, 25 km
22 Jan 03:00 UT	Esrange	67.8° N/21.1° E	18, 20, 23 km
22 Jan 21:00 UT	Esrange	67.8° N/21.1° E	18, 22, 25 km
23 Jan 11:00 UT	Esrange	67.8° N/21.1° E	19, 22, 25 km
23 Jan 19:00 UT	Esrange	67.8° N/21.1° E	19, 22, 25 km
24 Jan 16:00 UT	Esrange	67.8° N/21.1° E	19, 21, 22 km
03 Jan 18:00 UT	IRF Kiruna	67.8° N/20.4° E	19, 21, 23 km
04 Jan 19:00 UT	IRF Kiruna	67.8° N/20.4° E	19, 21, 26 km
06 Jan 20:00 UT	IRF Kiruna	67.8° N/20.4° E	18, 20, 22 km
08 Jan 02:00 UT	IRF Kiruna	67.8° N/20.4° E	20, 22, 24 km
11 Jan 21:00 UT	IRF Kiruna	67.8° N/20.4° E	25, 26, 27 km
12 Jan 21:00 UT	IRF Kiruna	67.8° N/20.4° E	22, 24, 26 km
13 Jan 00:00 UT	IRF Kiruna	67.8° N/20.4° E	22, 24, 26 km
14 Jan 20:00 UT	IRF Kiruna	67.8° N/20.4° E	22, 24, 26 km
16 Jan 01:00 UT	IRF Kiruna	67.8° N/20.4° E	22, 24, 26 km
17 Jan 01:00 UT	IRF Kiruna	67.8° N/20.4° E	20, 22, 24 km
22 Jan 06:00 UT	IRF Kiruna	67.8° N/20.4° E	18, 20, 25 km
23 Jan 20:00 UT	IRF Kiruna	67.8° N/20.4° E	20, 22, 24 km
23 Jan 05:00 UT	IRF Kiruna	67.8° N/20.4° E	18, 20, 22 km
24 Jan 17:00 UT	IRF Kiruna	67.8° N/20.4° E	19, 20, 22 km

**Denitrification and  
polar stratospheric  
cloud formation**

F. Khosrawi et al.

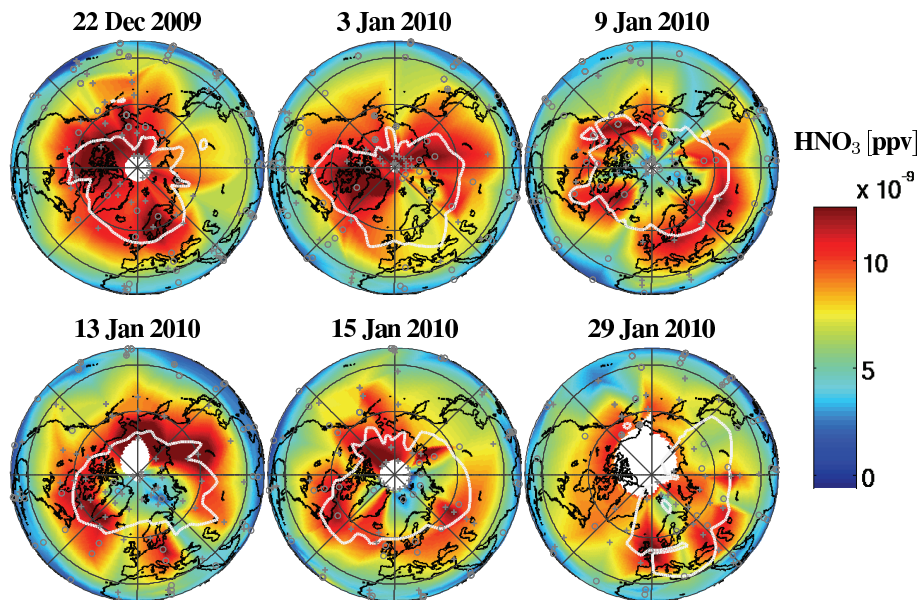


**Fig. 1.** Global distributions of  $\text{HNO}_3$  derived from Odin/SMR observations for the 22 December, 03, 09, 13, 15 and 29 January at 525 K. The white line is the 125 ppbv contour of  $\text{N}_2\text{O}$ , chosen to indicate the edge of the polar vortex.

Title Page

Abstract

Introduction

Conclusions

References

Tables

Figures

◀

▶

◀

▶

Back

Close

Full Screen / Esc

Printer-friendly Version

Interactive Discussion



**Denitrification and  
polar stratospheric  
cloud formation**

F. Khosrawi et al.

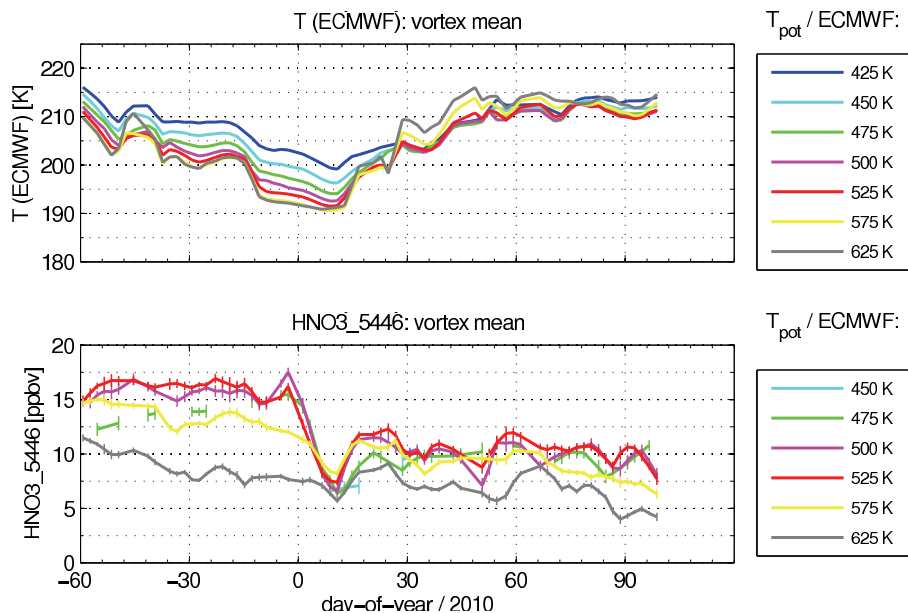


**Fig. 2.** Time series (vortex mean) of temperature derived from ECMWF (top) and HNO<sub>3</sub> (544.6 GHz band) derived from Odin/SMR (bottom) during the Arctic winter 2009/2010.

[Title Page](#)[Abstract](#)[Introduction](#)[Conclusions](#)[References](#)[Tables](#)[Figures](#)[◀](#)[▶](#)[◀](#)[▶](#)[Back](#)[Close](#)[Full Screen / Esc](#)[Printer-friendly Version](#)[Interactive Discussion](#)

## Denitrification and polar stratospheric cloud formation

F. Khosrawi et al.

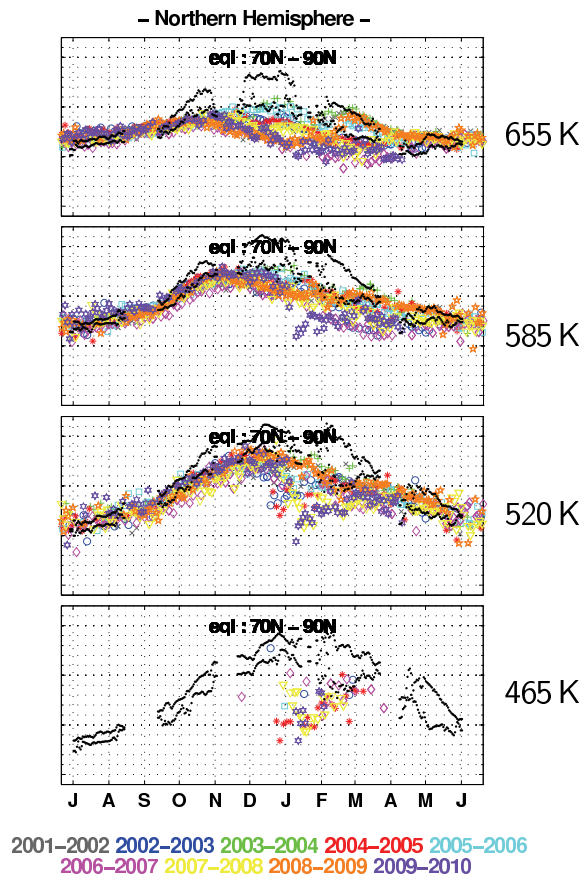


**Fig. 3.** Annual  $\text{HNO}_3$  variability derived from Odin/SMR observations at equivalent latitudes between  $70^\circ\text{N}$  and  $90^\circ\text{N}$  at potential temperature levels of 655, 585, 520 and 465 K for the Arctic winters 2001/2002 to 2009/2010 (color) and the climatological mean derived from UARS/MLS (1991–1998) observation (black) at these potential temperature levels.

**Denitrification and  
polar stratospheric  
cloud formation**

F. Khosrawi et al.

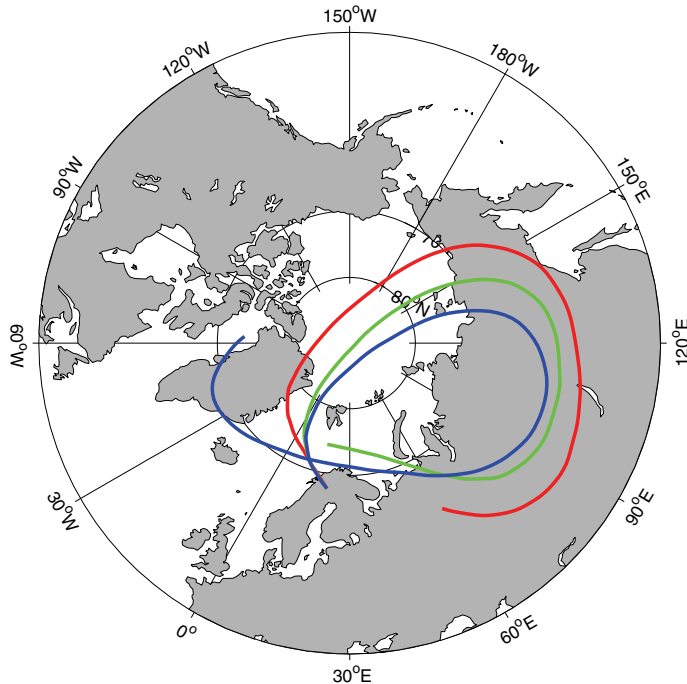


**Fig. 4.** Trajectories calculated 6-days backward starting at the ESRANGE (67.8° N, 21.1° E) for the measurements made on 23 January on 19:00 UT at three different altitude levels, 19 km (red), 22 km (green) and 25 km (blue).

Title Page

Abstract

Introduction

Conclusions

References

Tables

Figures

◀

▶

◀

▶

Back

Close

Full Screen / Esc

Printer-friendly Version

Interactive Discussion



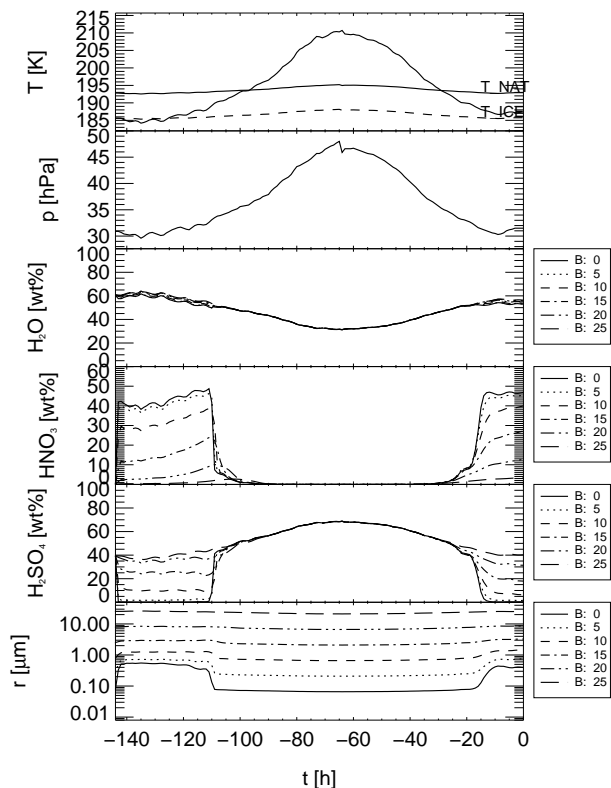


**Fig. 5.** Microphysical box model simulation for the observation at Erange on 22 January 19:00 UTC (22 km). Shown is the development of the temperature in K, the pressure in hPa, the weight fraction of water, nitric acid and sulfuric acid as well as the particle radius in  $\mu\text{m}$  for the different particle size classes denoted by B0–B25 (B0 = smallest and B25 = largest size class). Note: the simulations are performed forward in time, thus, the end of the simulation coincides with the measurement and the starting point of the trajectory.

## Denitrification and polar stratospheric cloud formation

F. Khosrawi et al.

Title Page

Abstract

Introduction

Conclusions

References

Tables

Figures



Back

Close

Full Screen / Esc

Printer-friendly Version

Interactive Discussion



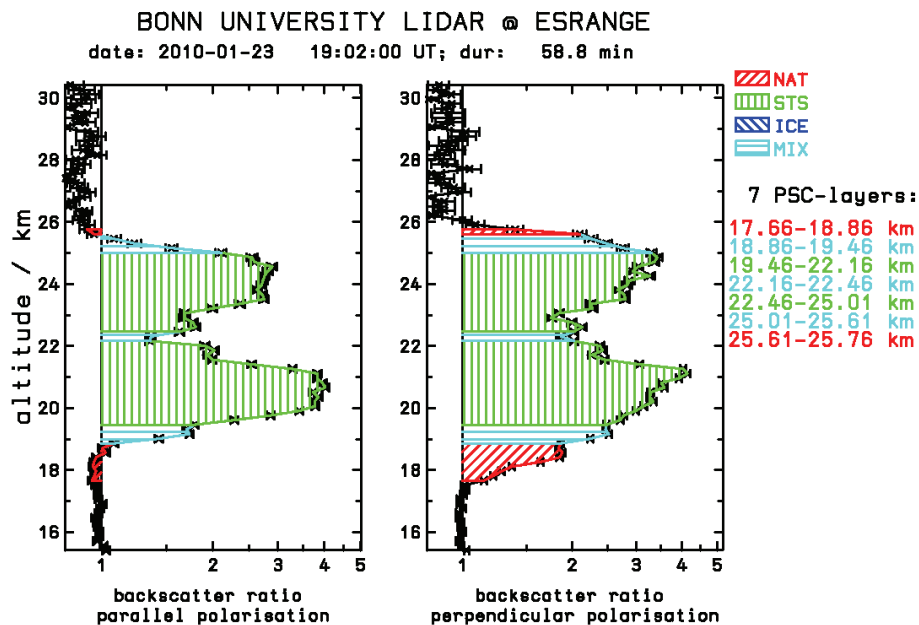


**Fig. 6.** Backscatter ratio in parallel (left) and perpendicular (right) polarisation measured with the Esrange lidar, 1-h integration time, starting at 19:02 on 23 January 2010. The colors mark the different PSC types.

## Denitrification and polar stratospheric cloud formation

F. Khosrawi et al.

Title Page

Abstract

Introduction

Conclusions

References

Tables

Figures

◀

▶

◀

▶

Back

Close

Full Screen / Esc

Printer-friendly Version

Interactive Discussion



## Denitrification and polar stratospheric cloud formation

F. Khosrawi et al.

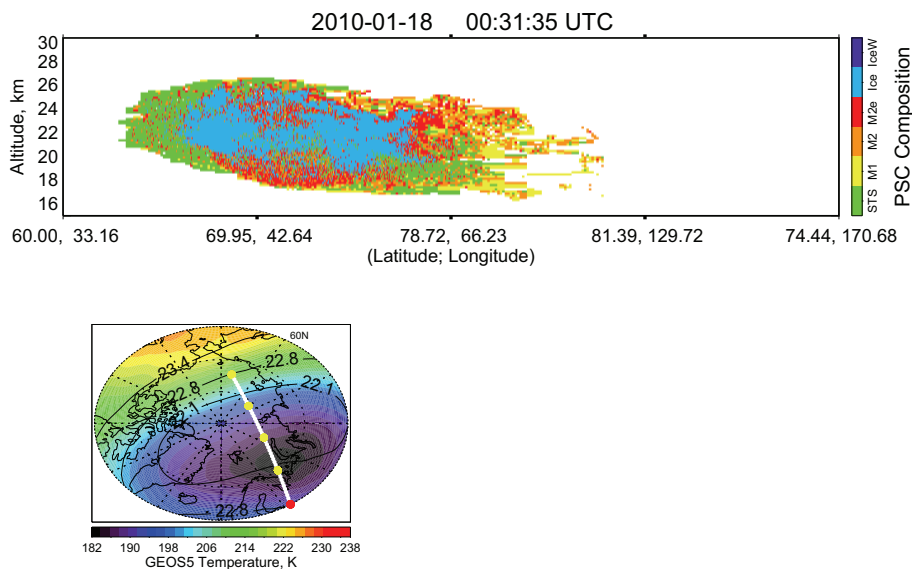


**Fig. 7.** CALIPSO PSC composition observation for the orbit starting on 18 January 2010 at 00:19 UTC (top) and GEOS-5 temperatures and geopotential height fields at 30 hPa at 12:00 UTC (right). The white line marks the CALIPSO orbit track.

Title Page

Abstract

Introduction

Conclusions

References

Tables

Figures

◀

▶

◀

▶

Back

Close

Full Screen / Esc

Printer-friendly Version

Interactive Discussion



**Denitrification and  
polar stratospheric  
cloud formation**

F. Khosrawi et al.

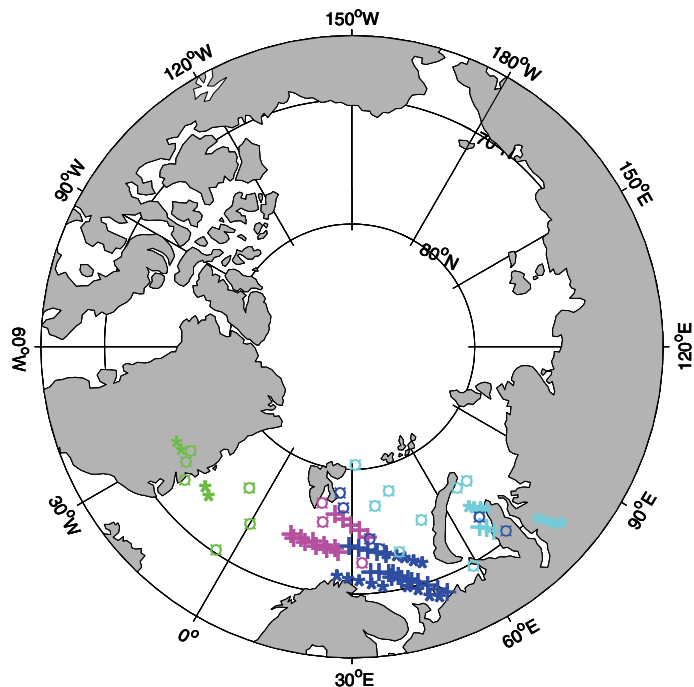


**Fig. 8.** The locations where  $T_{ice}$  along the back trajectories was encountered. The back trajectories that were started from IRF Kiruna are denoted with a star, the ones started from Esrange with a plus symbol and the CALIPSO measurements are denoted with circles. The dates when  $T_{ice}$  was encountered are colour coded: 2 January (green), 15 January (magenta), 17 January (dark blue) and 18 January (light blue).

Title Page

Abstract

Introduction

Conclusions

References

Tables

Figures

◀

▶

◀

▶

Back

Close

Full Screen / Esc

Printer-friendly Version

Interactive Discussion

